CHAPTER 2

GaN-Based Micro-Hole Array Light-Emitting Diodes

2.1 Progress in GaN-based Micro-Structure Device

Recent progress in electro-optical systems demands drastic increases in the degree of integration of photonic and electronic devices for large-capacity and ultrahigh-light output and information processing. Device size has to be scaled down to nanometric dimensions to meet this requirement, which will become even stricter in the feature. The success of the III-nitride light emitters, including blue light-emitting diodes (LEDs) and laser diodes (LDs) is encouraging for the investigation of microcavity lasers and micro-LEDs. New physical phenomena and properties begin to dominate as device size approaches the wavelength of light, including modified spontaneous emission, enhanced quantum efficiency, emission lifetime, the spectral linewidth, enhanced quantum efficiency, and reduced lasing threshold in microcavities, all of which warrant fundamental investigations [1-3]. In 1997, the optical properties of GaN/AlGaN multiple quantum well microdisks had been studied, which demonstrate strong enhancement of the transition intensity and lifetime in microdisk structures as shown in Fig. 2.1 and 2.2 [4]. Optical resonance modes in GaN pyramid microcavities and in III-nitride multiple quantum well microdisk/microring cavities were observed in 1998 and 1999, respectively [5-7]. Recently, the development of microdisplays has mainly focused on liquid crystal (LC), LC on silicon [8], and organic light-emitting diode (OLED) technologies [9]. Microdisplays are small displays that are of such high resolution that they can only be viewed or projected with lenses or mirrors.

The microsize LEDs and lasers provide benefits over edge emitters including the ability to fabricate arrays of individually controllable pixels on a single chip and enhanced quantum efficiency. Recently, H. W. Choi and H. X. Jiang *et al* have demonstrated a lot of III-nitride-based microsize optoelectronics such as matrix-addressable InGaN-based microdisplays (Fig. 2.3), GaN microdisk LEDs (Fig. 2.4), III-nitride blue microdisplays (Fig. 2.5), InGaN microring LEDs and high-density matrix-addressable AlInGaN-based 368-nm microarray LEDs etc (Fig. 2.6 and 2.7) [10-14]. A major imitation to the external quantum efficiency lies in the extraction efficiency of light from the device mesa structure. Such devices are opening up improvements in white LEDs for solid-state lighting applications, and are also expected to offer wide applicability in areas including high-density data storage, chemical and biological sensing devices, in sterilizers and as exposure tools for

photolithography. In a commercial photolithographic exposure system, to take one example, both the ultraviolet light source, which is currently typically a mercury lamp or a laser, and a mask for each pattern in a semiconductor device, are essential to the microfabrication. Since the light source and the mask are independent, it is not possible to correct any device failure due to a design error without making a new mask. In a word, The microsize LEDs have advantages of easy coupling to optical fibers and follow the integration of a dense two-dimensional array onto a single chip.

2.2 Design and Simulation of μ-Hole Array LEDs

InGaN-based quantum-well (QW) LEDs are affecting the development of full-color displays, illumination, and exterior automotive lighting over a spectral range from near ultraviolet to green and amber. Devices are grown epitaxially on either sapphire or silicon carbide substrates and their structure contains a single InGaN/GaN QW active region sandwiched between two GaN layers. The absorption coefficient of GaN in the photon-energy range from 2.0 to 3.1 eV is approximately 3×10^2 cm^{-1} [15], so some of the light from the active region is absorbed before it leaves out the devices. Furthermore, approximately $1/(4n^2)$ of the light from the active region radiates through the top and bottom of the devices because of guided modes in which light is totally reflected between the device surface and the air [16]. (The GaN refractive index n is ~2.4) Recently, III-nitride micro-LEDs (μ-LEDs) have attracted great interest in the area of high-extraction efficiency optoelectronic devices. Many groups have reported high-performance GaN-based micro-disk and micro-ring LEDs [17-21]. These μ-LEDs are generally accepted to have greater light output efficiencies than their broad-area (BA) conventional LED counterparts because the (re)absorption of light is reduced on the micrometer scale. Additionally, their greater extraction efficiency relative to the BA devices is attributable to the scattering of light from the etched sidewall surfaces and the great increase in the surface areas of the μ-LEDs [17]-[19]. However, the decline in the area of light-generation of the μ-LEDs may importantly affect their light output performance. This work focuses on the design, fabrication, and characteristics of InGaN-based LEDs μ-hole array LEDs. The effects of the decline in the area of the active region on light output by μ-hole array LEDs were also investigated in detail.

Extraction efficiency of conventional designs is limited by (as shown in Fig. 2.8)

- Light transmission through semi-transparent p-metallization,
- Absorption of wave-guided light due to multiple pass reflections,
- Light is obscured by bonding pads and wires, Light is obscured by bonding pads and

wires,

- Large dice are further limited by reduced side light escape. Large dice are further limited by reduced side light escape.

TracePro® is a general raytracing program for illumination analysis, optical analysis, radiometry analysis, and photometry analysis. It is the first optics software to be based on the industry-standard ACIS solid modeling kernel from Spatial, Inc. It is also the first software to combine true solid modeling, powerful optical analysis features, strong data exchange capabilities, and an enjoyable graphical interface. Fig. 2.9 shows an irradiance map of a conventional GaN-based LED of 360 × 250 μm^2 simulated from the Trace Pro program. From the Fig. 2.9 we can see that the output-light intensity is observed to be stronger at the edge of the device than that at the center of the device. In this study, the propagation and reflection of light in the devices were examined by applying the ray tracing method associated with the two-dimensional model in TracePro [22], [23]. The parameters used in all simulations of this work are shown in table 2.1. We designed a series of μ-hole array LEDs with hole-diameters of 3, 7, 11, and 15 μm and the spacing between two holes was fixed at 25 μm.

2.3 Fabrication of GaN-Based Micro-Hole Array LEDs

The examined samples were grown on c-plane sapphire substrates with a 30 nm-thick GaN nucleation layer by metalorganic chemical vapor deposition (MOCVD). The LED structure contains a 4 μm-thick Si-doped n-GaN; an active layer of five-period $In_{0.2}Ga_{0.8}N$ (3 nm)/GaN (7 nm) QWs; a 50 nm-thick Mg-doped $Al_{0.15}Ga_{0.75}N$ layer, and a 0.25 μm-thick Mg-doped p-GaN. Finally, samples topped with a contact layer of 50-pair Si-doped n^+-$In_{0.23}Ga_{0.77}N$/GaN short-period superlattices rather than high-resistivity p-GaN to reduce the p-contact resistance and improve the current spreading [24]. The wafer growth procedures are reported in detail elsewhere [25].

Figure 2.10 shows the processing of the InGaN-based micro-hole array LEDs which began with electron-beam evaporated Ni (5 nm)/Au (8 nm) to form a high-transparency p-type Ohmic contact [26]. The holes and the rectangular mesa (360 μm × 250 μm) were fabricated simultaneously by photolithographic patterning, the wet etching of Ni/Au layers and inductively coupled plasma (ICP) self-aligned dry etching (SAMCO ICP-RIE 101iPH). The dry etching was performed in a gas mixture of Cl_2/Ar = 10 /25 sccm with an ICP source power of 400 W, a bias power of 40 W and a chamber pressure of 5 mTorr. The effect of pattern-dependent etching on the micro-hole array LEDs is not obvious under these etching conditions. The samples were then etched down to the n-GaN layer with an approximate

depth of 1.2 μm. The diameters of the holes were 3, 7, 11, and 15 μm, as determined using a scanning electronic microscope (SEM) measurement. Figure 2.11 is a SEM image shows the etching result with d= 3 μm and spacing between two holes was fixed at 25 μm. Notably, the procedures for fabricating the micro-hole array LEDs are identical to those for fabricating conventional BA LEDs. Thermal annealing was applied to the p-type contact alloy at 500^{o}C in air for 5 minutes. Finally, the trilayers of Ti/Pt/Au (50 nm/20 nm/200 nm) for p-type pad were deposited. Figure 2.12 (a) shows an optical microphotograph of the top of a micro-hole array LED chip and d = 7 μm. Figure 2.12 (b) schematically depicts a micro-hole array LED. The conventional BA LEDs with the same mesa size (360 μm × 250 μm) were also fabricated from the same wafer for comparison. The probe-station system (Wentworth Laboratories, model: MP2300) is used for electronically characteristic measurements as shown in Fig. 2.13. The typical current-voltage measurements were performed using a high current measure unit (KEITHLEY 238). The light output power was measured using a calibrated power meter with a large Si detector (detector area 10×10 mm^2) approximate 5 mm above the device, collecting the light emitted in the forward direction.

2.4 Characteristics of GaN-Based Micro-Hole Array LEDs

Figure 2.14 plots the current-voltage (*I*-*V*) characteristics of the micro-hole array LEDs with different values of *d* and that of a conventional BA LED fabricated from the same wafer. The devices have unequal area of light-generation, so the insert in Fig. 2.14 plots the current density-voltage (*J*-*V*) (evaluated by taking the ratio of the actual driving currents to their active areas). The forward bias voltage, V_F, at a driving current of 20 mA increases with *d* (V_F = 3.38, 3.41, 3.57 and 3.80 V for *d* = 3, 7, 11 and 15 μm) and slightly exceeds that of the conventional BA LED (V_F = 3.28 V). The *J*-*V* characteristic is similar to the *I*-*V* characteristic in Fig. 2.14. Additionally, the operating voltages of the micro-hole array LEDs marginally exceed those of the conventional BA LED, because of the reduction in the total active area [17], [18], [27] and the presence of a plasma-damage region parallel to the sidewalls within the holes [28]. The holes were fabricated by dry etching; plasma damage occurs on the sidewalls, increasing the surface recombination of the injected electrons and holes.

Figure 2.15 plots the light output-current density (*L*-*J*) curves. The micro-hole array LED with *d* = 7 μm has a light output power of ~ 3.0 mW at 22.2 A/cm^2 (corresponding to a driving current of 20 mA for the conventional BA LED), which is 36% greater than ~ 2.2 mW for the conventional BA LED. Moreover, the light output power of the micro-hole array LEDs decreases as the *d* increases above 11 μm and the light output power of the micro-hole array

LED with d = 15 μm is less than that of the conventional BA LED. The insert in Fig. 2.15 plots the light output-current (*L-I*) curves. The light output power increases as the d increases, being distinct from the *L-J* curves. Notably, the *L-I* curves are similar as the d increases above 7 μm. The light output by an optoelectronic device is governed by the internal quantum efficiency and extraction efficiency. Internal quantum efficiency is a natural property of LEDs; the geometry of the device strongly influences the extraction efficiency. Figure 2.16 (a) and (b) present the emission image and the intensity profile of a micro-hole array LED with d = 7 μm at an operating current of 1 mA, respectively. A bright luminescence ring is observed at the periphery of the hole, similar to that observed in micro-pillar LEDs [17]. Figure 2.17 shows the schematic of light extraction of the BA and micro-hole array LEDs. Most of the light propagated in the plane is emitted through the surface of the sidewall, but scattering on the etched sidewall causes some of the light to be extracted from the top surface near the periphery, causing the ring of light to be observed in the emission images, and increasing the light output in the forward direction.

The propagation and reflection of light in the devices were examined by applying the ray tracing method associated with the two-dimensional model in TracePro [22], [23]. The emission power densities in the active regions of all devices were set identical in the simulation. Figure 2.18 plots the factor by which the light output power of various micro-hole array LEDs exceeds that of a conventional BA LED and the ratio (γ) of the etched (lose) light-generating-area of a micro-hole array LED to the mesa area of a conventional BA LED, as functions of d. The enhancement factor of the micro-hole array LED with d = 7 μm is ~ 39% and is similar to the experimental values, 36%, slightly exceeding it perhaps because non-radiative recombination on the etched sidewall surfaces of the micro-hole array LEDs. Additionally, in Fig. 2.18, the enhancement factor decreases as γ increases above 6% (d > 7 μm) and no enhancement is observed from the micro-hole array LEDs at γ > 28%. The large increase in the surface areas efficiently promotes the extraction of the photons that propagate in-plane and the scattering of light off of the sidewalls in the micro-holes. A fraction of the light-generating-area of the micro-hole array LEDs was etched, producing a less active region in the micro-hole array LEDs than that in the conventional BA LEDs. The competition between the improvement in light extraction and the reduction in the area of the active region importantly affects the light output. Accordingly, optimally designing micro-hole array LEDs considerably improves the light output efficiency.

In summary, highly efficient InGaN-based micro-hole array LEDs were fabricated. Their characteristics were measured and compared with those of conventional BA LEDs fabricated

from the same wafer. The light output from the micro-hole array LEDs was over 36% grater than that from conventional LEDs with the same device areas. In particular, microhole array LEDs exhibited no enhancement when $\gamma > 28\%$. These facts are attributable to combination of the enhancement in extraction efficiency by increasing the area of the sidewall surfaces and the reduction of the active areas of the micro-hole array LEDs. Optimally designed InGaN-based micro-hole array LEDs exhibit improved light output efficiently and are candidate for white-light LEDs or high-power/ high-efficiency large-area LEDs.

Table 2.1. Parameters for the light-tracing simulation of micro-hole array LEDs.

Refractive index (n)		Transmission of Ni/Au (%)	50
GaN	2.5	Total power from	
AlGaN	2.2	the active region (mW)	1
Air	1	Absorption coefficient	100
Sapphire	1.8	(λ = 460 nm, cm^{-1})	

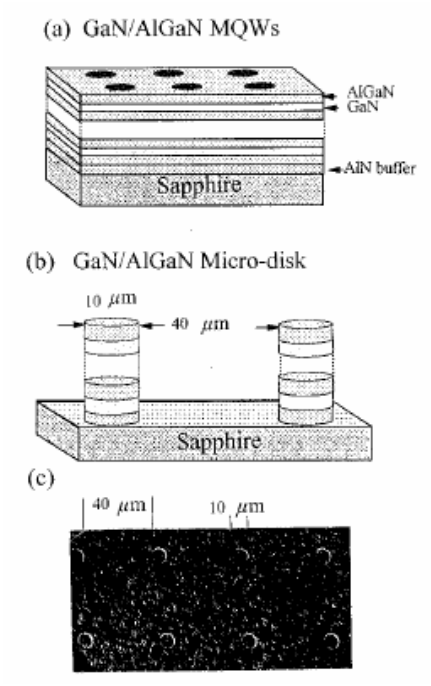

Fig. 2.1. Schematics of (a) the MQW structure and (b) the MQW microdisks. A top view SEM image of the microdisk structure is shown in (c). [4]

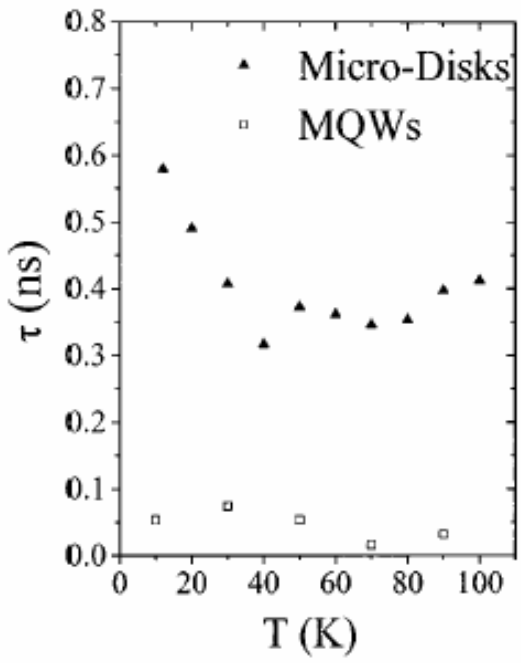

Fig. 2.2. Temperature dependence of the A-exciton decay lifetime (τ) up to 100 K. Open squares represent the MQWs and closed triangles represent the microdisks.

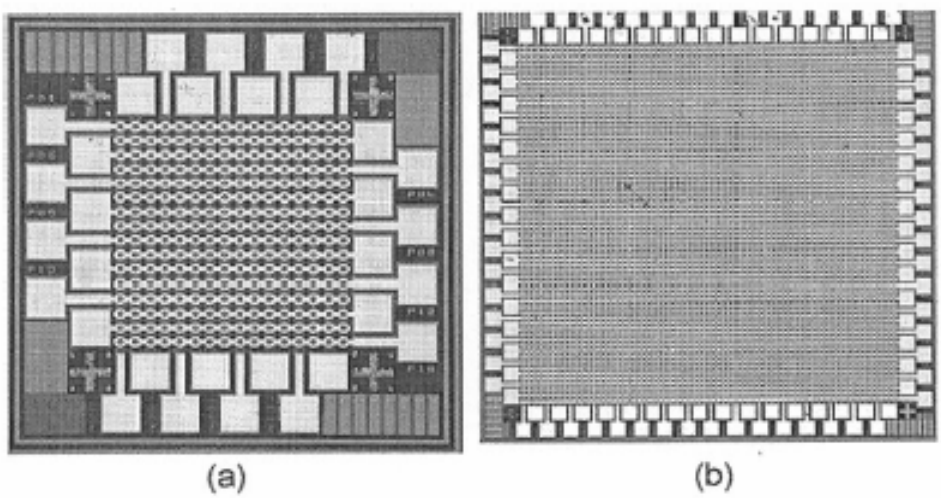

Fig. 2.3. Optical microphotographs of (a) 16 ×16 micro-LED array (the image is 0.9 mm on a side) and (b) 64 × 64 array (2.4 mm on a side).

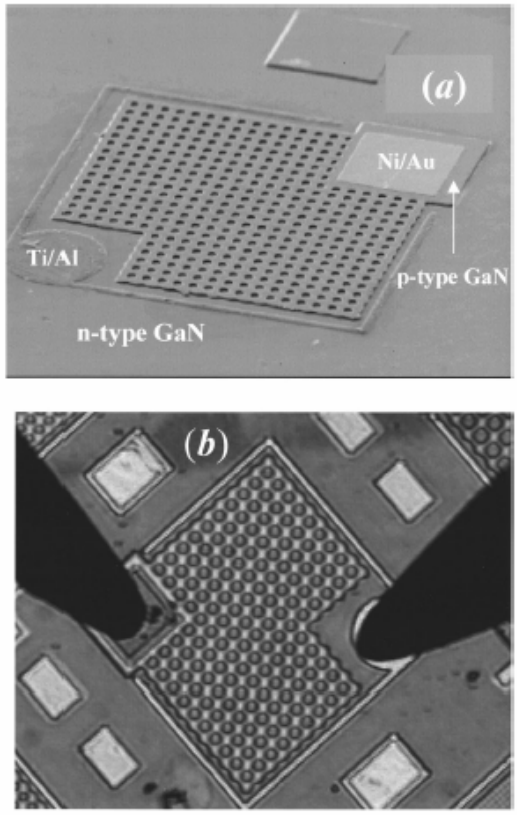

Fig. 2.4. (a) SEM and (b) optical microscope images of one of our interconnected μ-disk LEDs fabricated from InGaN/GaN QW structures. As illustrated in these images, about 200 μ-disk are interconnected and fit into an area of $300\times330\mu m^2$.

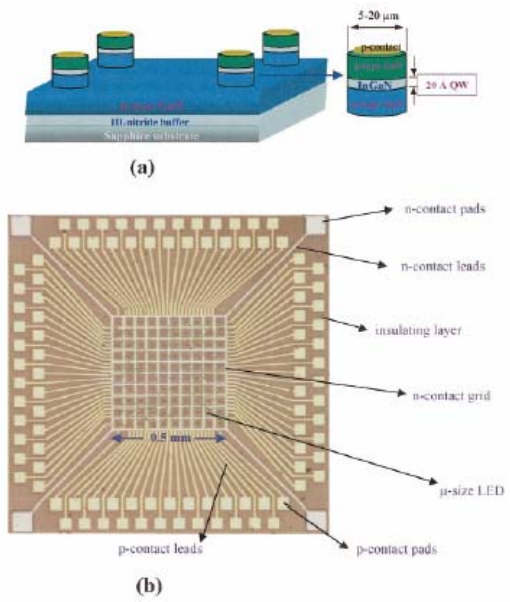

Fig. 2.5. (a)Schematic of μ-disk LEDs based on p-GaN/InGaN/n-GaN QWs. (b) Optical microscope image (top view) of a microdisplay fabricated from an individually addressed m-disk LED array. The dimension of the microdisplay is 0.5×0.5 mm^2 (made up of 10×10 pixels, 12 μm in diameter). [12]

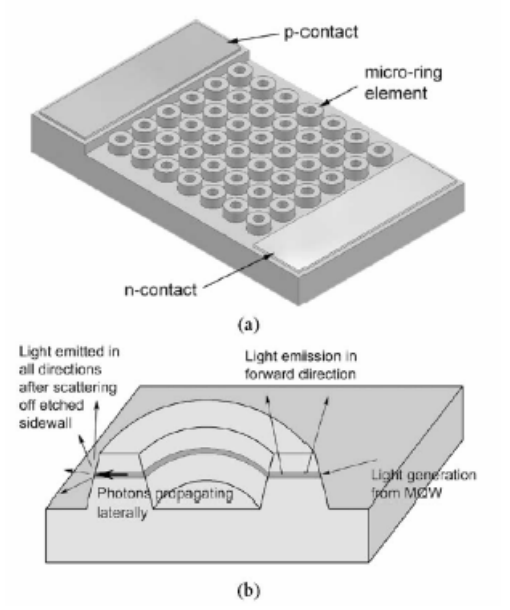

Fig. 2.6. (a)Schematics of the design of a microring LED and (b) diagram showing the possible light extraction pathways from a microring geometry.

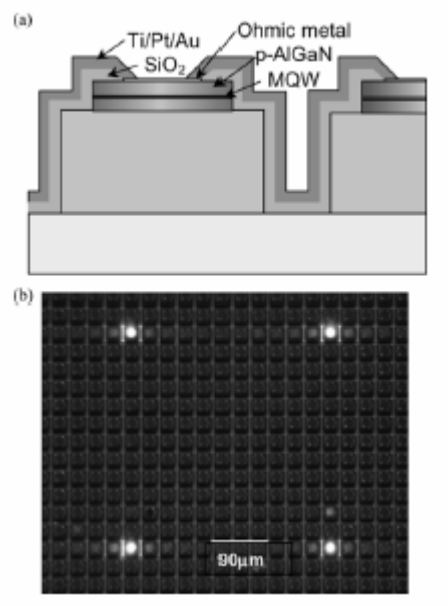

Fig. 2.7. (a) Cross-sectional schematic of the device structure, and (b) microscope image of the operating device showing four pixels turned on at 6 V.

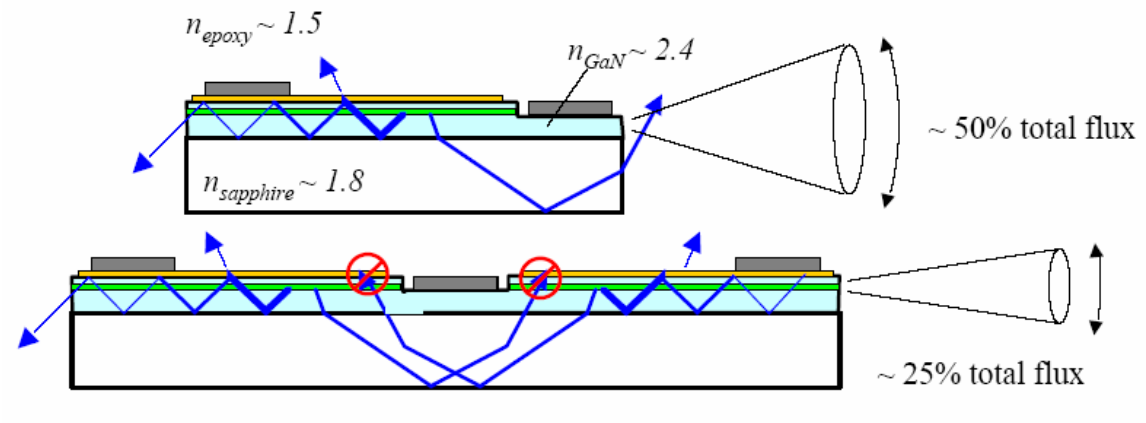

Fig. 2.8. Diagrams of extraction efficiency for the conventional LEDs.

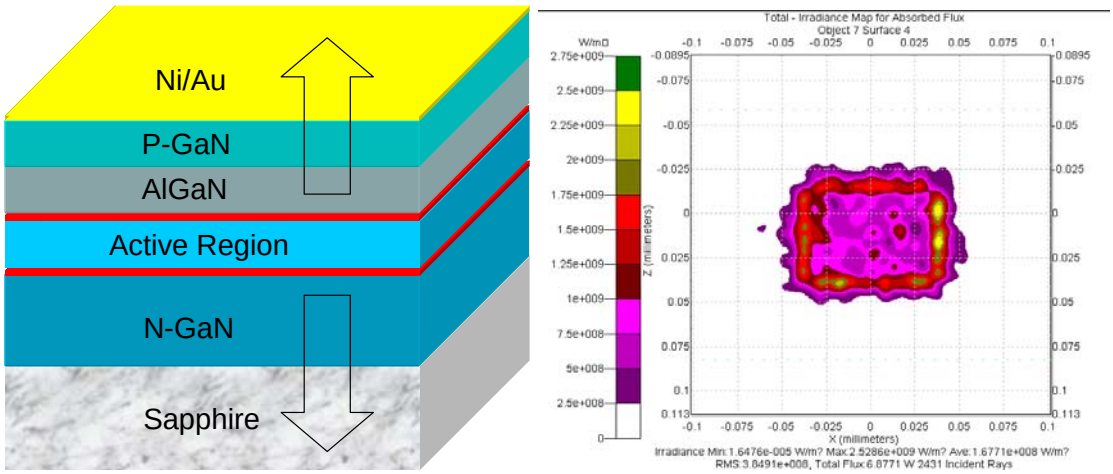

Fig. 2.9. Irradiance map of a conventional LED with device dimension of 360×250 μm^2 simulated from the Trace Pro program.

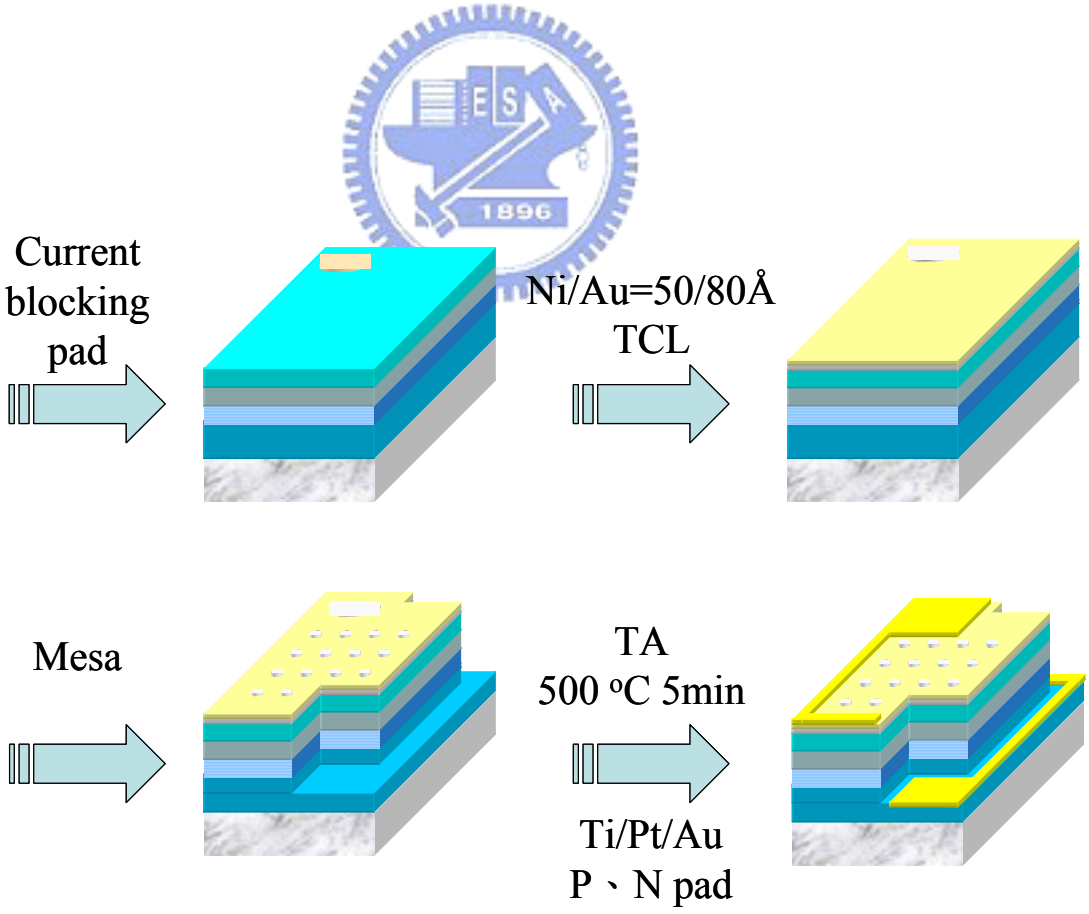

Fig. 2.10. Showing the process flowchart of the GaN-based micro-hole array LEDs.

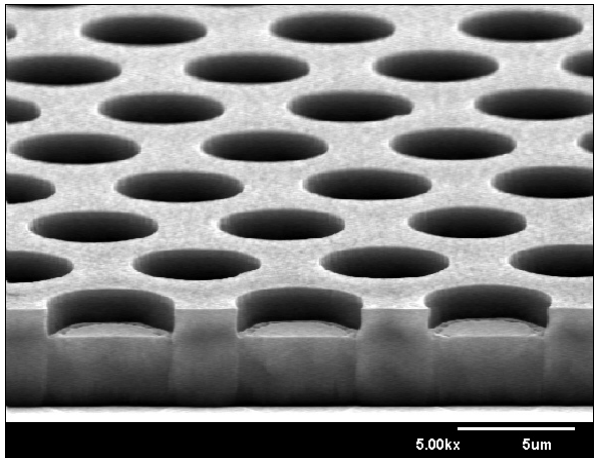

Fig. 2.11. Cress-sectional SEM image of the micro-hole array LED.

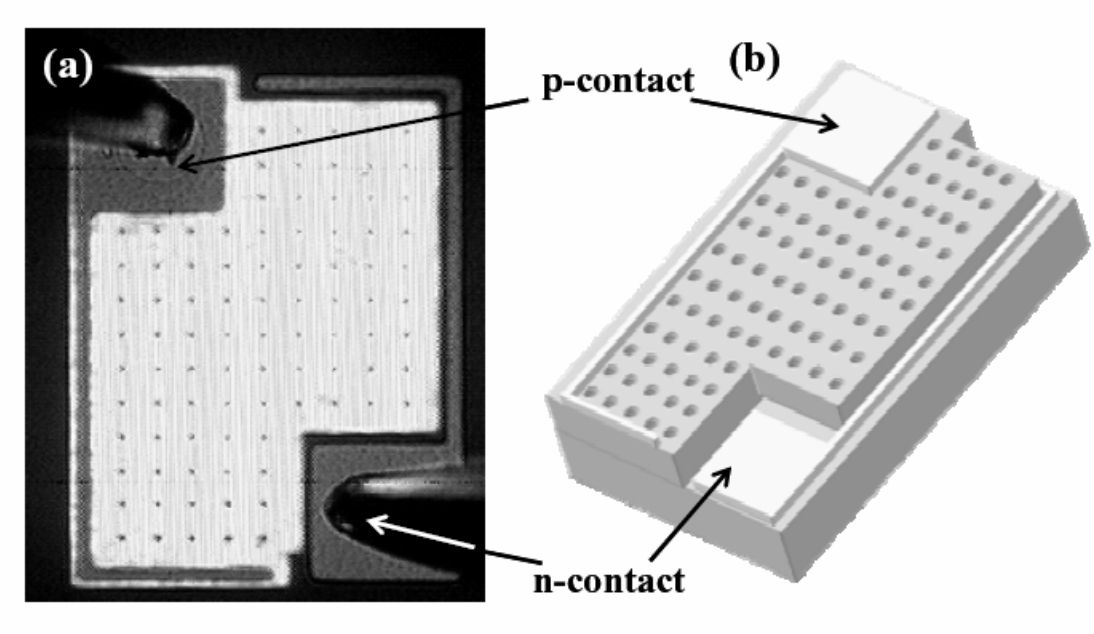

Fig. 2.12. Optical microscope image of a 360 μm × 250 μm micro-hole array LED with d = 7 μm. (b) schematic diagram of a representative micro-hole array LED fabricated by photolithography patterning and dry etching.

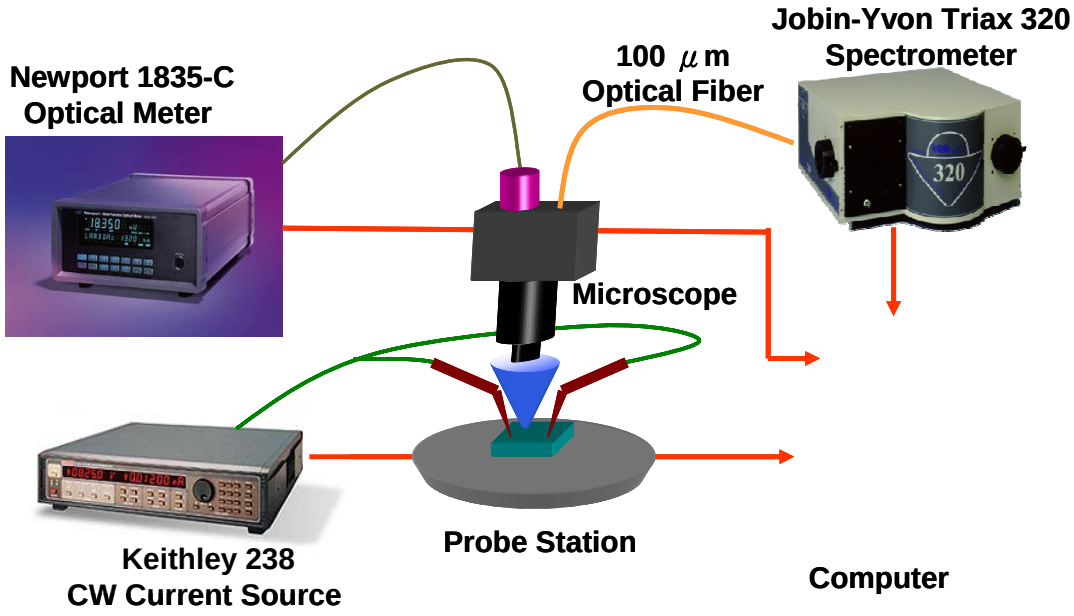

Fig. 2.13. Diagram of Electrical measurement system.

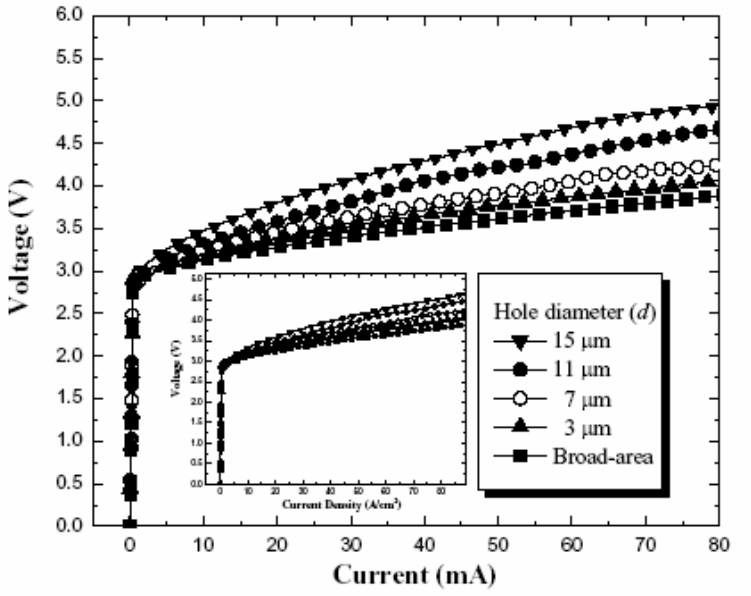

Fig. 2.14. Curves of current-voltage (*I*-*V*) of micro-hole array LEDs and a conventional BA LED fabricated from the same wafer. The insert is the current density-voltage (*J*-*V*) curves of the devices.

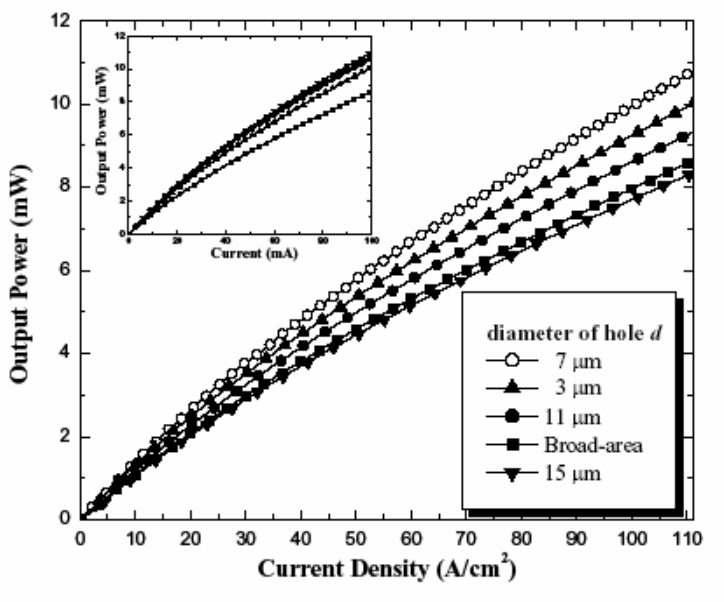

Fig. 2.15. Light output power of micro-hole array LEDs and a conventional BA LED as functions of injected current density. The insert shows the light output power-current (*L*-*I*) curves.

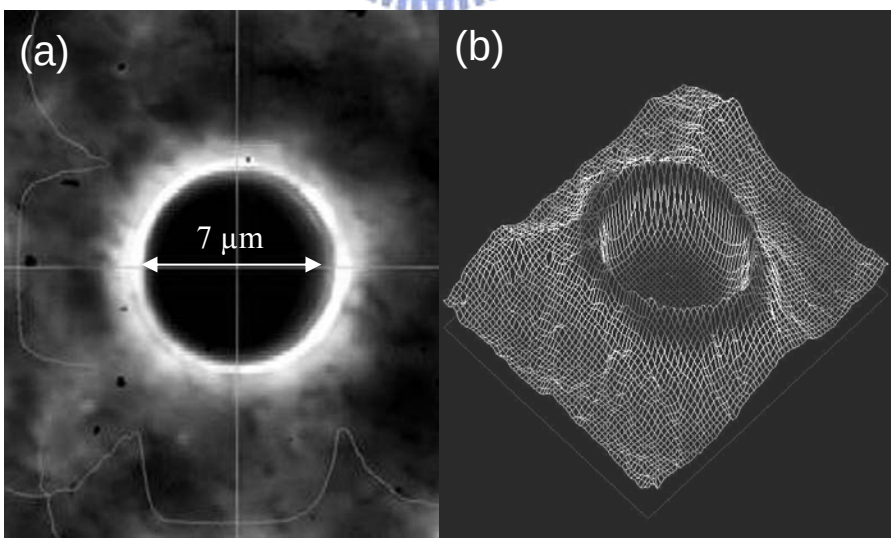

Fig. 2.16. Showing (a) micro-photograph and (b) emission profile of a micro-hole array LED with d = 7 μm at 1 mA driving current.

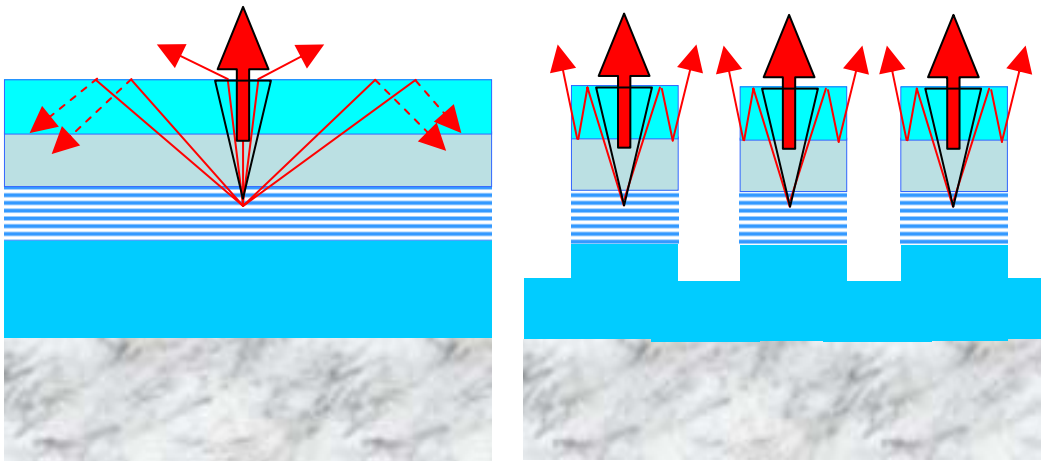

Fig. 2.17. Schematic of light extraction in BA and micro-hole array LEDs.

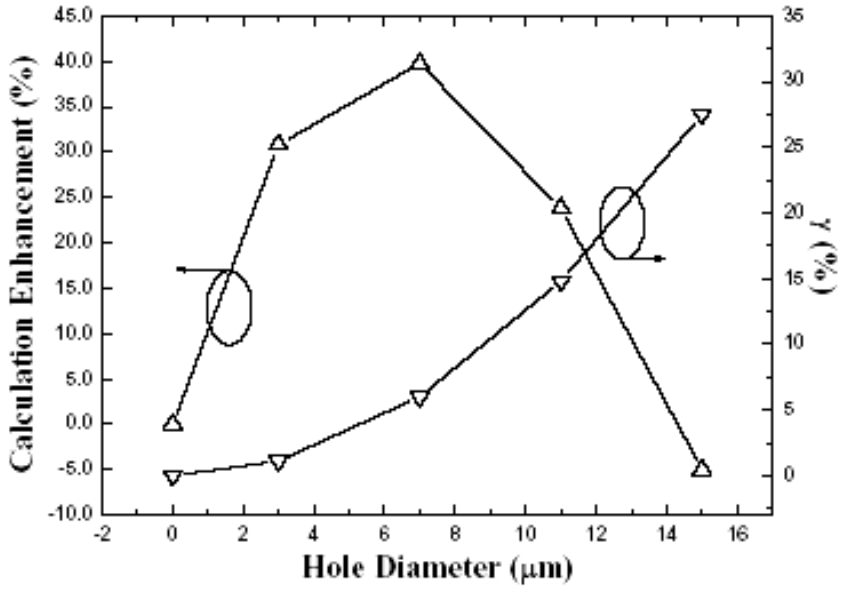

Fig. 2.18. Showing the calculation enhancement of light output power from the micro-hole array LEDs (simulation) and the γ, as functions of *d*.

REFERENCE

[1] R. K. Chang and A. J. Campillo, Optical Processes in Microcavities, World Scientific, Singapore (1996).
[2] R. A. Mair, K. C. Zeng, J. Y. Lin, H. X. Jiang, B. Zhang, L. Dai, A. Botchkarev, W. Kim, H. Morkoc, and M. A. Khan, Appl. Phys. Lett. 72, 1530 (1998).
[3] K. C. Zeng, L. Dai, J. Y. Lin, and H. X. Jiang, Appl. Phys. Lett. 75, 2563 (1999).
[4] R. A. Mair, K. C. Zeng, J. Y. Lin, H. X. Jiang, B. Zhang, L. Dai, H. Tang, A. Botchkarev, W. Kim, and H. Morkoc, Appl. Phys. Lett. 71, 2898 (1997).
[5] R. A. Mair, K. C. Zeng, J. Y. Lin, H. X. Jiang, B. Zhang, L. Dai, A. Botchkarev, W. Kim, H. Morkoc, and M. A. Khan, Appl. Phys. Lett. 72, 1530 (1998).
[6] H. X. Jiang, J. Y. Lin, K. C. Zeng, and W. Yang, Appl. Phys. Lett. 75, 763 (1999).
[7] K. C. Zeng, L. Dai, J. Y. Lin, and H. X. Jiang, Appl. Phys. Lett. 75, 2563 (1999).
[8] H. W. Kwok, "Development of liquid crystal on silicon microdisplays," in Proc. 7th Int. Display Workshop, Tokyo, Japan and San Jose, CA, 11-14 (2000).
[9] O. Prache, "Active matrix molecular OLED microdisplays, "Displays, 22, 49 (2001).
[10] C. W. Jeon, H. W. Choi, and M. D. Dawson, IEEE Photonics Tech. Lett. 15, 1516 (2003).
[11] S. X. Jin, J. Li, J. Z. Li, J. Y. Lin, and H. X. Jiang, Appl. Phys. Letts 76, 631 (2000).
[12] H. X. Jiang, S. X. Jin, J. Li, J. Shakya, and J. Y. Lin, Appl. Phys. Lett. 78, 1303 (2001).
[13] H. W. Choi, C. W. Jeon, and M. D. Dawson, IEEE Photonics Tech. Lett. 16, 33 (2004).
[14] C. W. Jeon, H. W. Choi, E. Gu, and M. D. Dawson, IEEE Photonics Technology. Lett. 16, 2421 (2004).
[15] O. Ambacher, W. Rieger, P. Ansmann, H. Angerer, T. D. Moustakas and M. Stutzmann, Solid State Communications 97, 365 (1996).
[16] M. Broditsk y and E. Yablonovitch, "Light-emitting diode extraction efficiency," Proc. SPIE, 3002, 119 (1997).
[17] S. X. Jin, J. Li, J. Y. Lin, and H. X. Jiang, Appl. Phys. Lett. 77, 3236 (2000).
[18] H. W. Choi, C. W. Jeon, and M. D. Dawson, IEEE Photonics Technology Lett. 16, 33 (2004).
[19] H. W. Choi, C. W. Jeon, M. D. Dawson, P. R. Edward, R. W. Martin, and S. Tripathy, J. Appl. Phys. 93, 5978 (2003).
[20] R. A. Mair, K. C. Zeng, J. Y. Lin, H. X. Jiang, B. Zhang, L. Dai, H. Tang, A. Botchkarev, W. Kim, and H. Morkoc, Appl. Phys. Lett. 71, 2898 (1997).
[21] K. C. Zeng, L. Dai, J. Y. Lin, and H. X. Jiang, Appl. Phys. Lett. 75, 2563 (1999).
[22] D. Eisert, and V. Harle, "Simulations in the Development Process of GaN-based LEDs and Laser Diodes," International Conference on numerical simulation of semiconductor optoelectronic devices, (2002).
[23] C. C. Kao, H. C. Kuo, H. W. Huang, J. T. Chu, Y. C. Peng, Y. L. Hsieh, C. Y. Luo, and S. C. Wang, C. C. Yu, C. F. Lin, IEEE Photonics Technology Lett. 17, 19 (2005).
[24] J. K. Sheu, G. C. Chi, and M. J. Jou, IEEE Electron Device Lett. 22, 160 (2001).
[25] S. J. Chang, C. S. Chang, Y. K. Su, R. W. Chuang, W. C. Lai, C. H. Kuo, Y. P. Hsu, Y. C. Lin, S. C. Shei, H. M. Lo, J. C. Ke, and J. K. Sheu, IEEE Photonics Technology. Lett. 16, 1002 (2004).
[26] J. K. Sheu, Y. K. Su, G. C. Chi, P. L. Koh, M. J. Jou, C. M. Chang,, C. C. Liu, and W. C. Hung, Appl. Phys. Lett. 74, 2340 (1999).
[27] N. Blanc, P. Gueret, P. Buchmann, K. Datwyler, and P. Vettiger, Appl. Phys. Lett. 56, 2216 (1990).
[28] E. D. Haberer, M. Woods, A. Stonas, C. –H. Chen, S. Keller, M. Hansen, U. Mishra, S. DenBaars, J. Bowers, and E. L. Hu, Mater. Res. Soc. Symp. Proc. 639, G11.21 (2000).